

Molecular, supramolecular structure and catalytic activity of transition metal complexes of phenoxy acetic acid derivatives

Avijit Pramanik, Srinivas Abbina, Gopal Das *

Department of Chemistry, Indian Institute of Technology Guwahati, Guwahati 781 039, Assam, India

Received 7 February 2007; accepted 17 July 2007

Available online 28 August 2007

Abstract

Six mononuclear complexes $[M(L_1)_2(H_2O)_4]$ ($M = Co(II)$, **1a** and $M = Mn(II)$, **1b**), $[Cu(L_1)_2(H_2O)_2]$ (**1c**), $[Cu(L_1)_2(H_2O)(Py)_2]$ (**1d**), $[Cu(L_3)(H_2O)Cl] \cdot H_2O$ (**3a**) and $[Co(Sal)(H_2O)(Py)_3] \cdot 2ClO_4 \cdot H_2O$ (**3b**) of phenoxyacetic acid derivatives and Schiff base were determined by single crystal X-ray diffraction. The $Co(II)$ (**1a**) and $Mn(II)$ (**1b**) complexes are isomorphous. X-ray crystal structural analyses reveal that these coordination complexes form polymeric structure via formation of different types of hydrogen bonding and π -stacking interactions in solid. Thermal analysis along with the powder X-ray diffraction data of these complexes shows the importance of the coordinated and/or crystal water molecules in stabilizing the MOF structure. Complexes **1a**, **1c**, **3a** show marginal catalytic activity in the oxidation of olefins to epoxides in the presence of *i*-butyraldehyde and molecular oxygen.

© 2007 Elsevier Ltd. All rights reserved.

Keywords: Metallacycles; Hydrogen bonds; Crystal engineering; Metal–organic framework; Thermal analysis; Catalytic activity

1. Introduction

In recent years, the main focus of supramolecular and materials chemistry has been the area of coordination frameworks, which are also known as coordination polymers or metal–organic frameworks (MOF) [1–3]. The increasing interest in this field is justified not only by their potential application as functional materials [4–6] but also by intriguing structural diversities of the architectures [7–9]. Synthesis of MOF structures is an active area of research, as these compounds can be potentially useful in several contemporary problems [10–12]. Coordination frameworks are also significant from a structural chemistry perspective with new structural types being discovered as well as providing numerous examples of phenomena such as the interpenetration of networks [13]. By closely controlling the coordination environment, frameworks with desir-

able structures and properties can be created. Thus, the prospect of tuning the properties of metal–organic frameworks through a systematic change of the coordination environment provides an impetus to further research of metal–organic architectures. Similarly hydrogen bonded networks of organic molecules [14] or coordination complexes [15] can also lead to highly ordered 2-D and 3-D structures. A well-known example of an organic functional group that forms hydrogen bonded network structures is carboxylic acid [16–19]. Carboxylate ligands can bridge two or more different metal centers and produce neutral architectures. These structures can be rapidly and conveniently built [20,21] using the modular or tinkertoy approach where topology of multidentate ligands as well as the coordination characteristics of the metal ions direct the self-assembly process.

We have previously demonstrated that tripodal ligand bearing carboxylic acid group can act as a mononuclear building block for the formation of an extended MOF [22,23]. The present investigation is an extension of the

* Corresponding author. Tel.: +91 3612582313; fax: +91 3612582349.
E-mail address: gdas@iitg.ernet.in (G. Das).

above studies in which the phenoxy acetic acid derivatives (**HL**₁, **HL**₂ and **HL**₃) with carboxylate groups to form extended solid state structures has been explored. We reported herein the six mixed-ligand mononuclear complexes of Cu(II), Co(II), Co(III) and Mn(II).

2. Experimental

2.1. Materials and methods

The aldehydes and the liquid olefins were distilled prior to use. Metal salts and solid olefins are used as supplied from commercial sources. All the solvents were purified prior to use by standard procedure. The IR spectra were recorded on a *Perkin–Elmer–Spectrum One* FT-IR Spectrometer with KBr disks in the range 4000–400 cm⁻¹. The thermo gravimetric analyses (TGA) of the compounds were performed by using an *SDTA 851e TGA* thermal analyzer (Mettler Toledo) with a heating rate of 2 °C per min in a N₂ atmosphere. Optical spectra were recorded in CH₃CN on a *Perkin–Elmer–Lambda 25-UV–Visible Spectrometer* at 298 K. Solid-state magnetic susceptibility of the complexes at room temperature was recorded using *Sherwood Scientific balance MSB-1*. Solution electrical conductivity measurements measured with a *Systronics Conductivity meter 306*. Elemental analyses were done using *Carlo Erba 1108* and *Perkin–Elmer series II 2400* instrument. GCMS analyses were performed using a *Perkin–Elmer Clarus 500* gas chromatograph coupled with the *Perkin–Elmer Clarus 500* mass spectrometer.

2.2. Synthesis of ligands **HL**_{1–3}

Both the ligands (Scheme 1) (4-formyl-phenoxy)-acetic acid (**HL**₁) [24] and (2-formyl-phenoxy)-acetic acid (**HL**₂) [25] were synthesized following the reported procedure.

2.2.1. Synthesis of ligands **HL**₃

To a stirred solution of **HL**₂ (111 mg, 0.5 mmol) in MeOH (10 ml) was added ethylene diamine (30 mg, 0.5 mmol) in MeOH (2 ml) at ice-cold condition. Mixture was then refluxed for 15 min and then allowed to cool to RT. Slow evaporation results the formation of yellow crystals, which was washed several times with cold MeOH. Yield 65%, m.p.: 186 °C; ESI-MS, *m/z* (%): 222 (86) [**HL**₃]⁺; *Anal. Calc.* for C₁₁H₁₄N₂O₃: C, 59.45; H, 6.35; N, 12.60. Found: C, 59.63; H, 6.31; N 12.55%. ¹H NMR (400 MHz, CDCl₃, 25 °C, TMS) δ (ppm): 3.2 (*t*, 2H), 3.8 (*t*, 2H), 4.7 (*s*, 2H), 6.8–7.6 (*m*, 4H), 8.2 (*s*, 1H), ¹³C

NMR (100 MHz, CDCl₃, 25 °C, TMS) δ (ppm): 42.8, 58.3, 79.8, 116.8, 121.5, 123.7, 131.2, 132.6, 161.4, 165.2, 174.1. FT-IR (KBr): 3442 ν(OH); 3351 ν(NH₂); 1765 ν(C=O); 1602 ν(C=N); 1490 ν(C=C); 1164 ν(COC) cm⁻¹.

2.3. Synthesis of complexes

2.3.1. Synthesis of [Co(L₁)₂(H₂O)₄] (**1a**)

To a stirred solution of **HL**₁ (18 mg, 0.1 mmol) in MeOH (5 ml) was added CoCl₂·6H₂O (23.8 mg, 0.1 mmol) in water (5 ml) at RT. The resulting solution was continued to stir for another 30 min. Slow evaporation of the reaction mixture afforded the complex **1a** as red crystals. These were employed directly for the X-ray crystallographic study. Yield: 85%, *Anal. Calc.* for CoC₁₈H₂₂O₁₂: C, 44.18; H, 4.53; Co, 12.04. Found: C, 44.24; H, 4.51; Co, 12.11%. Molar conductance (in CH₃CN): 4.1 S cm² mol⁻¹; solid-state RT μ_{eff} = 5.22 BM; UV–Vis: 456 nm (sh) [⁴A_{1g} → ⁴A_{2g}(F)], 511 nm [⁴T_{1g}(F) → ⁴T_{1g}(P)].

2.3.2. Synthesis of [Mn(L₁)₂(H₂O)₄] (**1b**)

Complex **1b** was synthesized following the same procedure as **1a**, only MnCl₂·4H₂O (20 mg, 0.1 mmol) was used instead of Co-salt. A light pink colored crystal of **1b** was studied by X-ray crystallography. Yield: 78%. *Anal. Calc.* for MnC₁₈H₂₂O₁₂: C, 44.54; H, 4.56; Mn, 11.32. Found: C, 44.51; H, 4.52; Mn, 11.39%. Solid-state RT μ_{eff} = 5.91.

2.3.3. Synthesis of [Cu(L₁)₂(H₂O)₂] (**1c**)

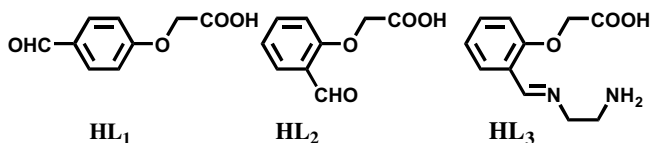
Complex **1c** was synthesized following the same procedure as **1a**, only CuCl₂·2H₂O (27 mg, 0.2 mmol) was used instead of Co-salt. A blue colored crystal of **1c** was studied by X-ray crystallography. Yield: 55%. *Anal. Calc.* for CuC₁₈H₁₈O₁₀: C, 47.21; H, 3.96; Cu, 13.87. Found: C, 47.17; H, 3.99; Cu, 13.92%; UV–Vis: 720 nm [²E → ²T₂], 900 nm (sh).

2.3.4. Synthesis of [Cu(L₁)₂(H₂O)(Py)₂] (**1d**)

Complex **1d** was synthesized following the same procedure as **1c**, only pyridine (24 mg, 0.3 mmol) was added after addition of metal salt solution and stirring was continued for additional 45 min in a closed container at RT. Dark blue crystal of **1d** was studied by X-ray crystallography. Yield: 42%. *Anal. Calc.* for CuC₃₀H₂₆N₂O₉: C, 57.92; H, 4.21; N, 4.50; Cu, 10.21. Found: C, 57.96; H, 4.25; N 4.46; Cu, 10.27%.

2.3.5. Synthesis of [Cu(L₃)(H₂O)Cl]·H₂O (**3a**)

To a stirred solution of **HL**₃ (11 mg, 0.05 mmol) in MeOH (3 ml) was added CuCl₂·2H₂O (7 mg, 0.05 mmol) in water (5 ml) at RT. The resulting solution was refluxed with continues stirring for another 15 min. The mixture was cooled to RT and slow evaporation of the reaction mixture afforded the complex **3a** as blue crystals. These crystals were used directly for the X-ray crystallographic study. Yield: 52%. *Anal. Calc.* for CuC₁₁H₁₈N₂O₅Cl: C,



Scheme 1. The phenoxy acetic acid derivatives **HL**₁, **HL**₂ and **HL**₃.

36.97; H, 5.07; N, 7.84; Cu, 17.78. Found: C, 36.91; H, 5.02; N, 7.91; Cu, 17.72%.

2.3.6. Synthesis of $[Co(Sal)(H_2O)(Py)_3] \cdot 2ClO_4 \cdot H_2O$ (**3b**)

To a stirred solution of **HL**₃ (11 mg, 0.05 mmol) in MeOH (3 ml) was added $Co(ClO_4)_2 \cdot 6H_2O$ (18.3 mg, 0.05 mmol) in water (5 ml) at RT. After 45 min of stirring at RT, excesses pyridine was added to this mixture. The resulting mixture was continued to stir for additional 45 min in a closed container at $\sim 60^\circ C$. Green crystal of **3b** was studied by X-ray crystallography. The perchlorate salts must be handled with care as this form potentially explosive mixtures with organic compounds. Yield: 48%. Anal. Calc. for $CoC_{25}H_{24}N_3O_{12}Cl_2$: C, 43.62; H, 3.51; N, 6.10; Co, 8.56. Found: C, 43.66; H, 3.54; N 6.17; Co, 8.51%; UV–Vis: 648 nm (ϵ 101 $M^{-1} cm^{-1}$) and 364 nm (ϵ 1420 $M^{-1} cm^{-1}$).

2.4. X-ray crystallography

The intensity data were collected using a Bruker SMART APEX-II CCD diffractometer, equipped with a fine focus 1.75 kW sealed tube Mo $K\alpha$ radiation ($\lambda = 0.71073 \text{ \AA}$) at 273(3) K, with increasing ω (width of 0.3° per frame) at a scan speed of 3 s/frame. The SMART software was used for data acquisition. Data integration and reduction were undertaken with SAINT and XPREP [26] software. Multi-scan empirical absorption corrections were applied to the data using the program SADABS [27]. Structures were solved by direct methods using SHELXS-97 [28] and refined with full-matrix least squares on F^2 using SHELXL-97 [28].

All non-hydrogen atoms were refined anisotropically. Most of the hydrogen atoms were located from the difference Fourier maps and refined isotropically. While other hydrogen atoms are added in a fixed geometry. Selected crystallographic data summarized in Table 1.

3. Results and discussion

3.1. Crystal structure of $[Co(L_1)_2(H_2O)_4]$ (**1a**) and $[Mn(L_1)_2(H_2O)_4]$ (**1b**)

The complexes **1a** and **1b** were crystallized from methanol/water (1:1) mixture as red and pink colored crystals respectively. The molecular structures with atom numbering scheme of the Co(II) complex (**1a**) and Mn(II) complex

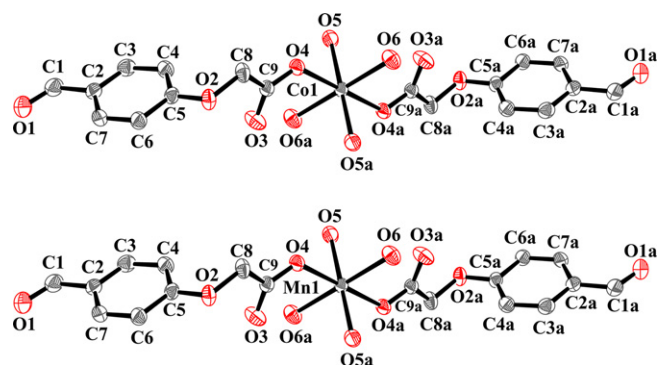


Fig. 1. ORTEP plot of complexes **1a** and **1b** with atom numbering scheme. Selected bond lengths for **1a**: Co(1)–O(4) = 2.1424(10), Co(1)–O(5) = 2.1029(14), Co(1)–O(6) = 2.0841(13); **1b**: Mn(1)–O(4) = 2.2301(9), Mn(1)–O(5) = 2.2018(12), Mn(1)–O(6) = 2.1596(12).

Table 1
Crystallographic refinement parameters of complexes **1a–3b**

Parameters	1a	1b	1c	1d	3a	3b
Empirical formula	$C_{18}H_{22}CoO_{12}$	$C_{18}H_{22}MnO_{12}$	$C_{18}H_{18}CuO_{10}$	$C_{28}H_{26}CuN_2O_9$	$C_{11}H_{17}ClCuN_2O_5$	$C_{22}H_{14}ClCoN_3O_8$
CCDC number	616704	616709	616707	616706	616708	616705
Fw	489.29	485.30	457.87	598.06	356.27	552.82
Temperature (K)	298(2)	298(2)	298(2)	298(2)	298(2)	298(2)
Radiation	Mo $K\alpha$	Mo $K\alpha$	Mo $K\alpha$	Mo $K\alpha$	Mo $K\alpha$	Mo $K\alpha$
Wavelength (\AA)	0.71073	0.71073	0.71073	0.71073	0.71073	0.71073
Crystal system	monoclinic	monoclinic	triclinic	monoclinic	orthorhombic	monoclinic
Space group	$P2_1/c$	$P2_1/c$	$P\bar{1}$	$C2/c$	$Pbca$	$C2/c$
<i>a</i> (\AA)	13.1134(4)	13.2560(2)	5.1099(6)	15.0747(9)	7.4235(17)	11.6418(3)
<i>b</i> (\AA)	9.8258(3)	9.86910(10)	7.0884(9)	5.9673(3)	18.289(4)	24.3575(7)
<i>c</i> (\AA)	8.0525(2)	8.10040(10)	13.0500(17)	30.8247(17)	21.406(5)	17.9014(5)
α ($^\circ$)	90.00	90.00	80.172(3)	90.00	90.00	90.00
β ($^\circ$)	106.2470(10)	106.4830(10)	87.763(3)	98.996(4)	90.00	94.838(2)
γ ($^\circ$)	90.00	90.00	77.215(3)	90.00	90.00	90.00
<i>V</i> (\AA^3)	996.13(5)	1016.18(2)	454.20(10)	2738.7(3)	2902.4(11)	5058.1(2)
<i>Z</i>	2	2	1	4	8	8
μ	0.932	0.709	1.260	0.849	1.698	0.827
<i>F</i> (000)	392	446	235	1188	1337	3248
Goodness-of-fit (S)	1.040	0.948	0.982	0.974	0.959	1.164
Final <i>R</i> indices	$R_1 = 0.0307$	$R_1 = 0.0301$	$R_1 = 0.0311$	$R_1 = 0.0436$	$R_1 = 0.0569$	$R_1 = 0.0551$
$[I > 2\sigma(I)]$	$wR_2 = 0.0481$	$wR_2 = 0.1071$	$wR_2 = 0.1046$	$wR_2 = 0.1117$	$wR_2 = 0.1365$	$wR_2 = 0.1660$
<i>R</i> indices (all data)	$R_1 = 0.0415$	$R_1 = 0.0356$	$R_1 = 0.0318$	$R_1 = 0.0788$	$R_1 = 0.0874$	$R_1 = 0.0979$
	$wR_2 = 0.493$	$wR_2 = 0.1157$	$wR_2 = 0.1057$	$wR_2 = 0.1300$	$wR_2 = 0.1607$	$wR_2 = 0.1913$

(**1b**) are shown in Fig. 1. Single-crystal X-ray analyses revealed both **1a** and **1b** are neutral and mononuclear in nature. In both the complex, metal ion is in similar coordination environment and each of them exhibits an octahedral geometry with MO_6 coordination. Bond angles and distances of mononuclear complex indicate a slightly distorted octahedral coordination with *trans*-geometry. Among the six O atoms around the metal ion, two carboxylate oxygen atoms are of ligand L_1 and four oxygen atoms are from water molecules. Metal bound four water molecules form the equatorial planes and L_1 is bonded in the axial positions. The little elongation of the M–O4 bond lengths agree with the bulkier nature of the ligand compared to the water molecules. The Co(II)/Mn(II) atom lies on a centre-of-inversion in the crystal structure. All the O atoms of the water and the Co or Mn atom lie exactly on the O_4 plane.

As shown in Fig. 1, carboxylate act as a uni-dentate ligand. In the crystal lattice, the coordinated water molecules are in two different environments within the 3D network. One set of water molecules has chelate type intramolecular hydrogen bonding with carbonyl group of carboxylate. The other set is hydrogen bonded to aldehyde group in the *para* position. This results in the formation of hydrogen bonded 2D tape type network along crystallographic *a* axis (see Supporting information). In the 2D tape network, the two neighboring M(II) ions show a distance of 13.113 Å (in **1a**) and 13.256 Å (in **1b**). However, the distance between benzene ring is 5.908 Å (in **1a**) and 5.945 Å (in **1b**) and they form an oval-shaped metalocycle unit. Uncoordinated O3 atom of carboxylic acid is intramolecularly hydrogen bonded to the nearest coordinated water molecule. Due to this each axial M–O4 bond is slightly tilted towards the M–O6 bond ($\angle\text{O}(6a)\text{--Co}(1)\text{--O}(4) = 88.26$ and $\angle\text{O}(6a)\text{--Mn}(1)\text{--O}(4) = 87.92$). In addition to this, both the carboxylate oxygen atoms are intermolecularly hydrogen bonded to the neighboring coordinated water molecules. Overall hydrogen bonding results the formation of staircase network viewed along crystallographic *a* axis (Fig. 2), Individual molecule is arranged in zig-zag fashion and helps to make the alternate steps of the staircase network.

The IR spectrum of complex **1a** shows typical antisymmetric and symmetric stretching bands of carboxylate groups at 1710 and 1280 cm^{-1} , respectively. The separation (Δ) between $\nu_{\text{asym}}(\text{CO}_2)$ and $\nu_{\text{sym}}(\text{CO}_2)$ is 430 cm^{-1} , indicating the presence of uni-dentate coordination modes in **1a**

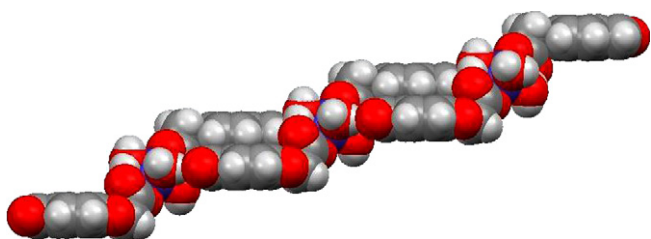


Fig. 2. Stair case network of **1a** along *a* axis.

[29]. This result is in good agreement with the crystal structure analysis. The OH stretching for water appearing at 3571 cm^{-1} and 3483 cm^{-1} shows that there are two different types of environment for water molecules.

Solid-state arrangement of complex **1b** is similar to that of **1a**, they are isostructural. The Mn–O bond distances for equatorially coordinated hetero atoms are typical for Mn(II) octahedral complexes [30,31]. It also shows the formation of similar 2D hydrogen bonded tape as well as the 3D stair case network viewed along *a* axis. The separation (Δ) between $\nu_{\text{asym}}(\text{CO}_2)$ and $\nu_{\text{sym}}(\text{CO}_2)$ is 405 cm^{-1} in the IR spectrum of **1b**, which also confirms the uni-dentate binding nature of the carboxylic acid group. In both the complex, the overall structure is stabilized by several weaker C–H \cdots O and C–H \cdots π interactions in addition to the stronger O–H \cdots O hydrogen bonding (see Supporting information). Complex **1b** is very faint pink in color and have no absorption bands in the visible region, in accordance with the high-spin d^5 electronic configuration of the Mn(II) ion. This complex is very stable in spite of being based on Mn(II). They may be stored in normal laboratory atmosphere without taking any precautions for more than two months.

3.2. Crystal structure of $[\text{Cu}(\text{L}_1)_2(\text{H}_2\text{O})_2]$ (**1c**) and $[\text{Cu}(\text{L}_1)_2(\text{H}_2\text{O})(\text{Py})_2]$ (**1d**)

The molecular structures with atom numbering scheme of both the Cu(II) complexes **1c** and **1d** are shown in Fig. 3.

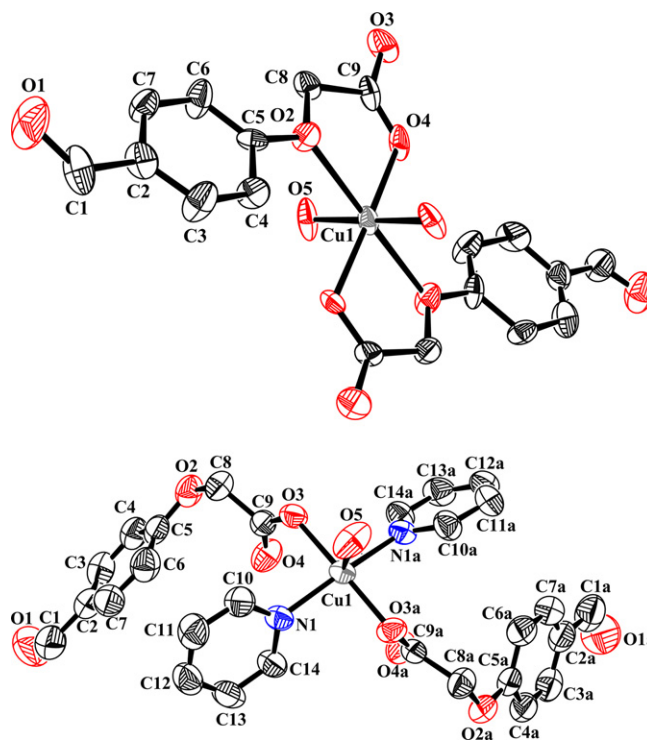


Fig. 3. ORTEP plot of complexes **1c** and **1d**. Selected bond lengths for **1c**: Cu(1)–O(2) = 2.4141(14), Cu(1)–O(4) = 1.9487(15), Cu(1)–O(5) = 1.9457(15); **1d**: Cu(1)–N(1) = 2.015(3), Cu(1)–O(3) = 1.962(2), Cu(1)–O(5) = 2.184(3).

In complex **1c** the Cu(II) atom is in the MO_6 coordination environment. It is ligated by six oxygen atoms: two carboxylato oxygen and two ether oxygen from ligand L_1 and two oxygen from water molecules. The carboxylato oxygen atoms bonds more strongly with the Cu(II) than ether oxygen atoms. Complex **1c** has two five-membered O,O-chelate rings. Bond angles and distances of neutral, mononuclear complex indicate a slightly distorted octahedral coordination with *trans*-geometry. The bond distances and bond angles involving the metal ions are similar with the similar type of coordination environment [32,33]. The shortening of the Cu–O4 bond lengths agree with the stronger chelating ability of the carboxylate oxygen compared to ether oxygen atoms. Due to the formation of five-membered chelate rings both the axial bonds are inclined towards the carboxylate donor in the equatorial plane ($\angle O(3)–Cu(1)–O(10) = 88.6$ and $\angle O(7)–Cu(1)–O(6) = 74.70$). Carboxylate oxygen atoms and water molecules form the equatorial plane while weakly bonded ether oxygen atoms occupy the axial positions. Cu(II) atom exactly lie within the equatorial plane without any deviation from the plane. The strong $O–H \cdots O$ and weaker $C–H \cdots O$ and $C–H \cdots \pi$ type intermolecular hydrogen bonding play a major role in stabilizing the solid-state structure. Each carboxylate oxygen atom form hydrogen bond with coordinated water molecules, which result in the formation of 2D sheet of metallacycle along *b* axis (see supporting information). All the Cu atoms form linear arrays in all three directions. Shortest Cu–Cu distance in each layer of 2D sheet is 7.088 Å, while shortest Cu–Cu distance between layers is 13.050 Å. Adjacent layers run in the same direction along the *b* axis. Each aldehyde oxygen forms two $C–H \cdots O$ type bond which leads to the formation of 3D double-staircase network in solid-state (Fig. 4). The $\nu(COC)$ band near 1105 cm^{-1} is shifted by 35 cm^{-1} in the FT-IR spectrum of complex **1c** to a lower frequency than the free ligand, which is also confirmed from X-ray structure analysis. Carboxylic acid is uni-dentate ligand here also, which shows the separation (Δ) between $\nu_{\text{asym}}(CO_2)$ and $\nu_{\text{sym}}(CO_2)$ stretching frequency of 395 cm^{-1} . Solid-state magnetic moment of **1c** is 1.85 BM. This value is consistent with a Cu(II) complex having an octahedral coordination geometry [34,35].

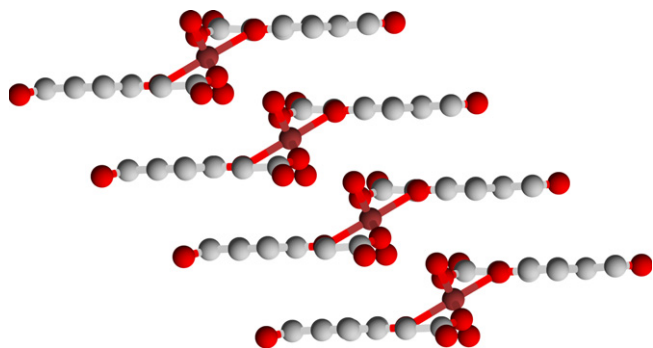


Fig. 4. Double-staircase network along *b* axis in **1c**.

Weaker coordination of the ether oxygen to the Cu(II) centre is lost, when stronger coordinating ligand pyridine is added during complex preparation. Complex **1d** crystallizes as a neutral monomer. The overall coordination environment changes from distorted octahedral to square pyramidal with *trans* geometry (Fig. 3), where the O atom of the water occupies the axial position. Square plane is formed by N_2O_2 coordination from L_1 and pyridine molecules. In this complex also, L_1 ligand coordinates to the copper in a uni-dentate fashion. Selected bond length and bond angles confirm the slightly distorted square pyramidal mononuclear Cu(II) complex. The equatorial Cu–O and Cu–N bond lengths are comparable with square-pyramidal CuN_2O_3 coordination spheres [36,37]. The axial Cu–O(5) bond length (2.184(3) Å) is consistent with the trend observed in other square-pyramidal Cu(II) complexes [38]. Cu(II) lies in the N_2O_2 mean plane with out any deviation. Both the ligands are bent in the opposite direction with respect to the coordinated water molecule that results in the formation of V-shape architecture. Fig. 5 shows the formation of 2D tape structure along *b* axis via formation of strong $O–H \cdots O$ hydrogen bond between carboxylate oxygen and water molecule. Shortest Cu–Cu distance in the same plane is 8.106 Å whereas shortest Cu–Cu distance between adjacent planes is 15.412 Å. It is also interesting to note that the pyridine molecules in the basal plane are twisted such that they are inclined at an angle of 38.93° from a common plane. This puckering brings the carbonyl group of the carboxylic acid group to the proximity of a hydrogen atom present at the 3-position of a coordinated pyridine molecule, resulting in a weak $C–H \cdots O$ interaction in the lattice. Due to steric crowding, two basal pyridines do not remain in the same plane. Water molecules are arranged in opposite direction on adjacent layer *i.e.* adjacent layer propagate along *b* axis in the opposite direction. Adjacent 2D tape is connected through $C–H \cdots O$ type

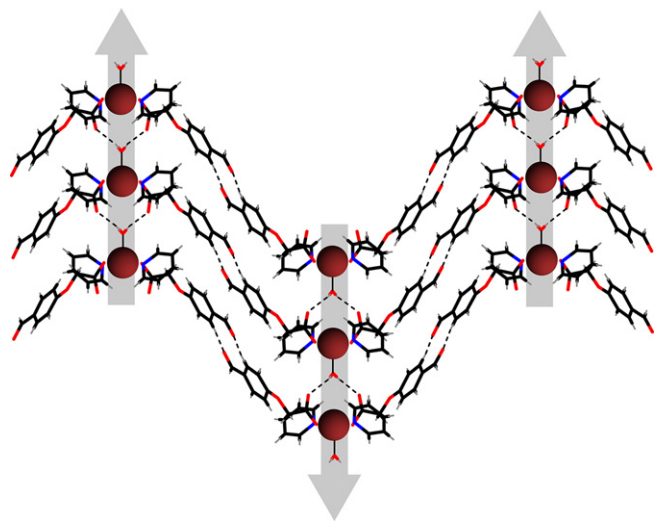


Fig. 5. Packing of **1d** along *b* axis showing $O–H \cdots O$ and $C–H \cdots O$ interactions.

hydrogen bond involving the aldehyde groups (Fig. 5). In contrast to the complex **1c**, benzene ring of the ligand in **1d** form π – π stacking interactions with another benzene ring in the adjacent layer. Upon complex formation in-plane ring deformation frequency of pyridine at 604 cm^{-1} is shifted to 643 cm^{-1} [39]. Although the electronic spectra of the copper complexes with multidentate Schiff base ligands are not in general good indicators of geometry [40], but act as supporter of it. The solid-state Nujol mull absorption spectrum for **1d** appeared at 650, 340 and 244 nm. The broad absorption band at 650 nm is attributable to a copper ion in square pyramidal chromophore CuN_2O_3 [41]. This broad visible absorption band at 650 nm is shifted slightly to a lower energy (678 nm) in acetonitrile solution, consistent with square pyramidal geometry in solution phase. The complex displays two strong absorption bands at 340 and 244 nm in solid which are clearly $\sigma(\text{N}) \rightarrow \text{Cu}(\text{II})$ LMCT in origin and these two bands are shifted to 348 and 248 nm, respectively, in solution. The solid-state magnetic moment number for **1d** is 1.91, which is typical [42] of a discrete mononuclear $\text{Cu}(\text{II})$ complex.

3.3. Crystal structure of $[\text{Cu}(\text{L}_3)(\text{H}_2\text{O})\text{Cl}] \cdot \text{H}_2\text{O}$ (**3a**)

Complex **3a** crystallizes as a neutral monomer. The molecular structures with atom numbering scheme of the $\text{Cu}(\text{II})$ complex is shown in Fig. 6. In the complex $\text{Cu}(\text{II})$ atom is in the $\text{N}_2\text{O}_3\text{Cl}$ coordination environment. Here all six coordination site is occupied by six different coordination group. Three oxygen atoms ligate it: one carboxylato oxygen, one ether oxygen from ligand L_3 and one from water molecule. Two nitrogen atoms are from imine and primary amine groups. The carboxylato oxygen atoms

bonds more strongly with the $\text{Cu}(\text{II})$ than ether and water oxygen atoms. The geometry of the ligand forced the ether oxygen to form a bond with the $\text{Cu}(\text{II})$ in more strongly nature than water molecule, which is not common to our knowledge. Complex **3a** has two five-member O,O and N,N -chelate rings along with one six-member N,O -chelate ring. Bond angles and distances of this mixed-ligand mononuclear complex indicate a slightly distorted octahedral coordination [18]. Water oxygen atom and chloride ion occupy the axial positions. $\text{Cu}(\text{II})$ atom exactly lie within the N_2O_2 equatorial plane without any deviation from the plane. Due to the formation two five-member and one six-member chelate rings in the same side of the complex, both the axial bonds are inclined towards the benzene ring of the donor in the equatorial plane. Uncoordinated carboxylate oxygen form hydrogen bond with neighboring coordinated water molecule. Hydrogen of NH_2 group simultaneously forms hydrogen bond with coordinated carboxylate oxygen atom and crystal water molecule.

Chloride ion form relative weaker hydrogen bond with both coordinated and uncoordinated water molecules (see Supporting information). The conventional strong $\text{O}-\text{H} \cdots \text{O}$, $\text{N}-\text{H} \cdots \text{O}$ hydrogen bonding along with unconventional weaker $\text{C}-\text{H} \cdots \text{O}$, $\text{C}-\text{H} \cdots \text{Cl}$ type intermolecular hydrogen bonding and $\pi \cdots \pi$ interactions form 3D zig-zag network (Fig. 7). All the benzene rings of the ligand form continuous π -stacking along a axis. Overall network is formed by 2D sheet arrangement of metallacycle along a axis. All the Cu atoms form rectangular boxes when viewed along b axis with a $\text{Cu}-\text{Cu}$ distance of 9.347 \AA and 7.848 \AA , respectively. Each of the crystal water is acting as single acceptor and double donor, which stabilize the overall network.

In aqueous solution, complex has a λ_{max} value of 619 nm ($\epsilon = 46\text{ M}^{-1}\text{ cm}^{-1}$) in the visible region due to a d–d transition and a λ_{max} value of 244 nm ($\epsilon = 5055\text{ M}^{-1}\text{ cm}^{-1}$) in the UV region due to a LMCT transition. As these values are far from that of aqueous CuCl_2 at 819 nm, it is reasonable to assume that at least most of complex species of **3a** are not dissociated in solution.

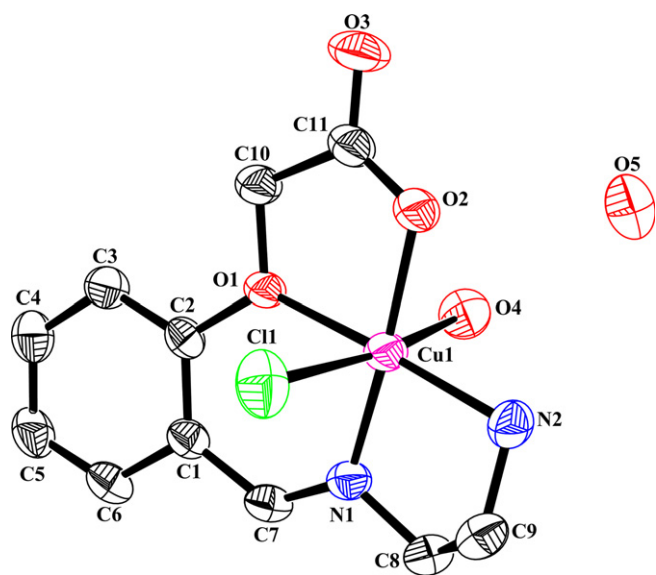


Fig. 6. ORTEP plot of Complex **3a**. Selected bond lengths are $\text{Cu}(1)-\text{O}(1) = 2.051(2)$, $\text{Cu}(1)-\text{O}(2) = 1.933(3)$, $\text{Cu}(1)-\text{O}(4) = 2.529(3)$, $\text{Cu}(1)-\text{Cl}(1) = 2.7102(12)$, $\text{Cu}(1)-\text{N}(1) = 1.940(3)$ and $\text{Cu}(1)-\text{N}(2) = 2.004(3)$.

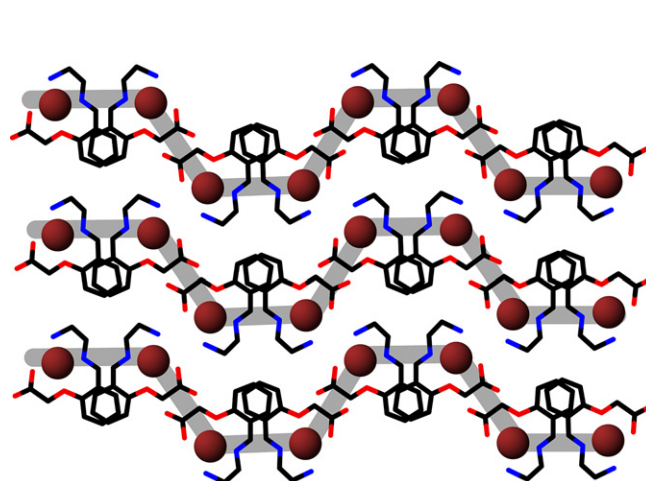


Fig. 7. Packing of **3a** along a axis.

3.4. Crystal structure

$[Co(Sal)(H_2O)(Py)_3] \cdot 2ClO_4 \cdot H_2O$ (**3b**)

When **L₃** was treated with $Co(ClO_4)_2$ salt in open atmosphere with subsequent treatment of excesses pyridine, we got salicylaldehyde Co(III) complex **3b**. Both the Schiff base and ether linkage has been cleaved and Co(II) is oxidized to Co(III) species during complex formation in open atmospheric condition. Unit cell contains one mononuclear Co(III) complex, one water and two perchlorate ions. Fig. 8 shows the ORTEP plot of complex **3b** without the counter anions. The geometry of the complex is distorted octahedral. Three pyridine nitrogen atoms and phenolate oxygen form the equatorial plane while axial positions are occupied by aldehyde and water oxygen. Pyridine molecules in the *trans* position are almost orthogonal to each other with a torsion angle $\angle C23-N4-N2-C10 = 86.10^\circ$. There is no deviation of Co(III) from N_3O basal plane. π -stacking interaction between pyridine rings forms the dimer.

Crystal water forms hydrogen bonds with two perchlorate anions and coordinated water molecule in single acceptor–double donor way. Overall metallacycle formed 2D MOF along *ab* plane by water and perchlorate anion (Fig. 9). Overall, 3D mosaic structure is obtained via formation of different types of hydrogen bonds (see Support-

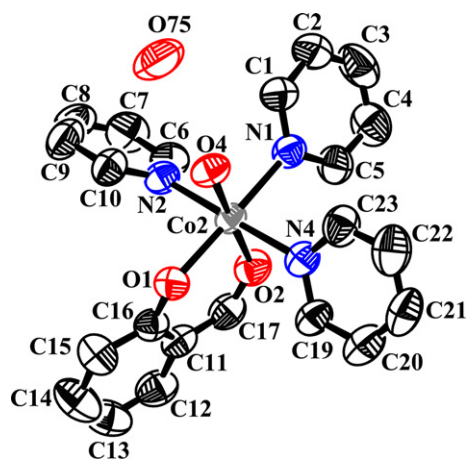


Fig. 8. ORTEP plot of complex **3b**, perchlorate anions are omitted for clarity. Selected bond lengths are $Co(2)-O(1) = 2.036(2)$, $Co(2)-O(2) = 2.055(2)$, $Co(2)-O(4) = 2.067(3)$, $Co(2)-N(1) = 2.124(3)$, $Co(2)-N(2) = 2.104(3)$, $Co(2)-N(4) = 2.105(3)$.

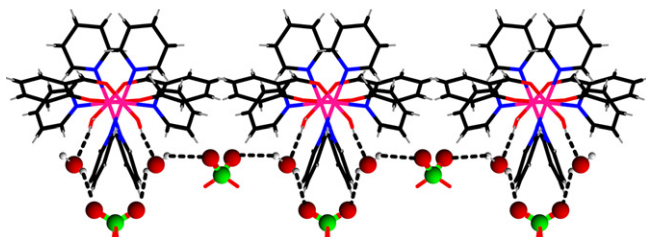


Fig. 9. Water and perchlorate assisted MOF along *ab* plane of **3b**.

ing information). All the Co(III) atoms form rectangular boxes along *b* axis with a Co–Co distance of 11.642 Å and 6.819 Å, respectively.

A strong peak in FT-IR spectrum of **3b** in 1625 cm^{-1} is attributable to the η^1 -bonded aldehyde ($C=O$) stretching vibrations. Another strong peak at 1118 cm^{-1} is attributed to the ClO_4^- ion.

3.5. Thermal and powder XRD analysis

Both **1a** and **1b** decomposed thermally in a number of steps. These complexes show successive thermal release of coordinated water molecules and the CO_2 followed by complete decomposition of the complex. The robustness of the framework is reflected in the thermo gravimetric analysis (TGA). TG analysis of complex **1a** in N_2 atmosphere shows the release of four coordinated water molecules ($50\text{--}150^\circ\text{C}$; $\Delta m = 14.66\%$ Calc.; 15.68% found) and two CO_2 molecules from the two coordinated carboxylate groups ($230\text{--}420^\circ\text{C}$; $\Delta m = 21.00\%$ Calc.; 20.93% found) (Fig. 10), which is in good agreement with the X-ray crystal structure. Complete decomposition is achieved at $\sim 600^\circ\text{C}$. The DSC-plot shows two endothermic peaks at 60°C and 100°C due to the loss of water molecules. It also shows two exothermic peaks at 260°C and 330°C due to the decomposition of the carboxylic acid groups. For complex **1b**, dehydration occurs at same temperature range that of **1a**, but decarboxylation occurs at $230\text{--}420^\circ\text{C}$.

Thermal analysis of complex **1c** shows 8.69% (calculated 7.82%) weight loss in the $120\text{--}180^\circ\text{C}$ due to the removal of two coordinated water molecules. It also shows the releases of two CO_2 molecules in the temperature range of $260\text{--}320^\circ\text{C}$ associated with 21.42% weight loss (calculated 20.75%). Complete decomposition takes place at 580°C . DSC profile shows two endothermic and one exothermic

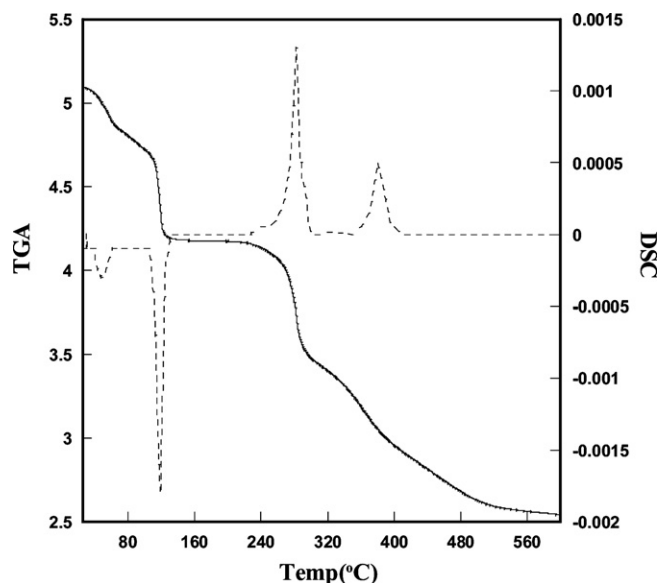


Fig. 10. TG–DSC curve of complex **1a**.

peak at 140 °C, 480 °C and 280 °C, respectively. TG analysis of **1d** exhibits a curve that corresponds to a weight loss of 28.88% (Calculated 21.17%) in the 110–190 °C range corresponds to the removal of one water, two pyridine and a further 21.42% (Calculated 20.75%) loss in the 300–490 °C temperature range, which corresponds to the release of two CO₂ molecules. DSC analysis shows one endothermic peak at 180 °C and one exothermic peak at 400 °C. Generally, a lattice water molecule is expected to be lost at a lower temperature. Thus, one would anticipate a loss of two water molecules of crystallization at a lower temperature than the coordinated water molecules in complex **3a**. TG analysis of complex **3a** in N₂ atmosphere shows the sequential release of crystal water (90–180 °C; $\Delta m = 5.05\%$ Calc.; 6.37% found) and coordinated water molecule (180–230 °C; $\Delta m = 5.32\%$ Calc.; 6.72% found). In the temperature range 300–410 °C it shows the release of chloride and one CO₂ ($\Delta m = 24.82\%$ Calc.; 36.47% found). The DSC-plot shows two endothermic peaks at 125 °C and 205 °C due to the loss of water molecules. It also shows two exothermic peaks at 470 °C and 500 °C. Thermal analysis was not performed with **3b** due to the presence of perchlorate salt.

PXRD patterns also confirm the crystalline nature of the complexes. PXRD patterns of **1a** show significant changes in the peak positions as well as intensities before and after water removal (Fig. 11). After heating the crystal of **1a** at 200 °C for 5 h in a muffle furnace, powder XRD was recorded. Loss of overall crystallinity after water removal confirms that the stability of MOF in the solid state is a result of the strong hydrogen bonding interactions involving coordinated water molecules. Similar observation was made with **1b** also. Complex **1b** was heated at

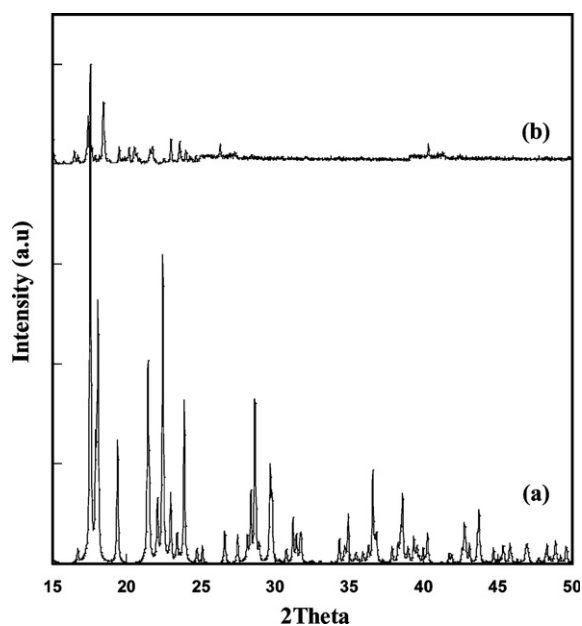


Fig. 11. Powder XRD pattern of complex **1a**. (a) Before water removal and (b) after water removal.

180 °C for 5 h in a muffle furnace to get rid of the coordinated water molecules. All the other complexes show the similar type of changes in the PXRD pattern before and after the removal of water molecules (see Supporting information).

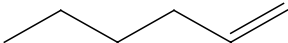
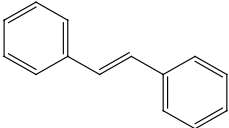
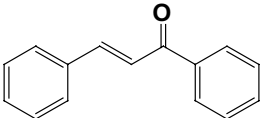
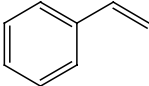
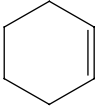
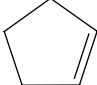
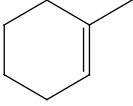
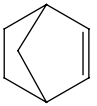
3.6. Catalytic activities of the complexes

All six water soluble complexes are tested as a catalyst in the epoxidation of linear and cyclic olefins under Mukaiyama's conditions [43]. It is found that only Co(II) complex **1a**, Cu(II) complexes **1c** and **3a** are found to be able to act as a catalyst in the epoxidation of alkenes by molecular oxygen in the presence of a sacrificial aldehyde, *i*-butyraldehyde [43–47] (Table 2). In all cases, blank tests performed in identical conditions but without metal catalyst gave negligible conversions of the substrates. It is interesting to note that the pyridine complexes (**1d**, **3b**) show very poor catalytic activity in the same reaction condition. Compared to the complexes **1a**, **1c** and **3a**, pyridine complexes required more reaction time and yielded less amount of product. In a typical experiment, a substrate (10 mmol) and *i*-butyraldehyde (20 mmol) were added to acetonitrile (15 ml) containing 5 mol% catalyst under an atmosphere of molecular oxygen at ambient pressure and temperature. TLC followed progress of the reaction. After completion or interruption of the reaction, the solid catalyst was filtered through a short plug of silica gel. The *i*-butyric acid formed is removed by washing with an aqueous NaHCO₃ solution. The excess of unreacted *i*-butyraldehyde is evaporated under vacuum together with the solvent. Aqueous workup followed by column chromatography afforded the corresponding epoxides. The epoxides were identified by comparison of their MS spectra and retention times in GC analysis with those of authentic samples. In absence of *i*-butyraldehyde, none of the complexes was able to cause epoxidation even if used stoichiometrically. This simple, environment friendly methodology has some drawbacks. It is not applicable to unreactive olefins. Yields are not quantitative. One has to invest stoichiometric amounts of *i*-butyraldehyde as a sacrificial reducer, whose role is that of an oxygen transfer agent. The likely mechanism is co-oxidation of the sacrificial aldehyde and the olefin. The mechanism can be compared with that of the reported in literature [47]. Detailed mechanisms of the catalytic processes are currently being investigated in our laboratory with some other acid–metal complexes, which are already published from our laboratory. A direct oxidation without using these catalysts *i.e.* the control reaction did not lead to any substantial oxidation product.

4. Conclusion

In conclusion, we report the synthesis and crystal structure of six mononuclear mixed-ligand complexes of phenoxycetic acid derivatives and Schiff base of Cu(II), Co(II)/(III), Mn(II). The carbonyl groups in the acetic acid

Table 2
Summary of catalyzed aerobic epoxidation of olefin

Entry	Olefin	Catalyst	Time (min)	Conversion (%)	Yield (%)
1		1a	45	95	58
		1c	20	98	64
		1d	480	71	33
		3a	20	98	68
		3b	300	67	28
2		1a	30	89	55
		1c	15	92	60
		1d	600	69	21
		3a	10	90	62
		3b	380	61	16
3		1a	50	94	52
		1c	30	97	68
		1d	420	66	31
		3a	15	98	65
		3b	240	70	23
4		1a	25	82	45
		1c	15	87	57
		1d	540	59	18
		3a	10	92	52
		3b	480	51	10
5		1a	20	92	48
		1c	10	96	58
		1d	360	62	26
		3a	10	98	63
		3b	240	56	17
6		1a	20	76	37
		1c	10	84	48
		1d	360	43	18
		3a	10	81	51
		3b	240	36	10
7		1a	30	94	52
		1c	25	98	63
		1d	420	58	21
		3a	20	98	71
		3b	300	47	14
8		1a	45	88	66
		1c	40	93	74
		1d	480	57	31
		3a	30	98	81
		3b	360	48	22

moiety provide the anchor to form two distinguishable sets of hydrogen-bonded motifs in all the complexes. It is interesting to note that carboxylic acid acts as a uni-dentate ligand in all the complexes. The Schiff base ligand has unique structure, which contains four different ligating atoms in one molecule. We have shown in the manuscript that ether oxygen can also bind to the metal center, which has very poor ligating capability. We demonstrated in the manuscript that the precise control of the coordination

environment of the metal center has an effect on the formation of 3D metallo-organic framework (MOF) in the solid state. 3D MOF structure has been critically analyzed and explained based on the monomer structure. We have tested the catalytic properties of all the metal complexes. We observed that subtle change in the coordination environment changes the catalytic properties drastically. Out of six complexes, **1c** and **3a** complexes shows marginal catalytic activities in the epoxidation of olefins by molecular

oxygen in the presence of *i*-butyraldehyde under Mukaiyama's conditions. We have not been able to observe addition or insertion of oxygen into the aromatic ring with any of these complexes.

Acknowledgements

The financial support from the Council of Scientific and Industrial Research (CSIR) of India to GD (Grant No. 01(1948)/04/EMR-II) is gratefully acknowledged. A.P. thanks CSIR for JRF. We thank Central Instrument Facility, Centre for Nanotechnology and Department of Chemistry IIT Guwahati for SEM, Powder XRD and Single crystal XRD measurements.

Appendix A. Supplementary material

CCDC 616704, 616709, 616707, 616706, 616708 and 616705 contain the supplementary crystallographic data for **1a**, **1b**, **1c**, **1d**, **3a** and **3b**. These data can be obtained free of charge via <http://www.ccdc.cam.ac.uk/conts/retrieving.html>, or from the Cambridge Crystallographic Data Centre, 12 Union Road, Cambridge CB2 1EZ, UK; fax: (+44) 1223-336-033; or e-mail: deposit@ccdc.cam.ac.uk. Supplementary data associated with this article can be found, in the online version, at [doi:10.1016/j.poly.2007.07.033](https://doi.org/10.1016/j.poly.2007.07.033).

References

- [1] J.M. Lehn, *Supramolecular Chemistry, Concepts and Perspectives*, VCH, Weinheim, 1995.
- [2] J.W. Steed, J.L. Atwood, *Supramolecular Chemistry*, Wiley, New York, 2000.
- [3] N.L. Rosi, J. Eckert, M. Eddaoudi, D.T. Vodak, J. Kim, M. O'Keeffe, O.M. Yaghi, *Science* 300 (2003) 1127.
- [4] C. Janlak, *J. Chem. Soc., Dalton Trans.* (2003) 2781.
- [5] C. Benelli, D. Gatteschi, *Chem. Rev.* 102 (2002) 2369.
- [6] J.S. Seo, D. Whang, H. Lee, S.I. Jun, J. Oh, Y.J. Jeon, K. Kim, *Nature* 404 (2000) 982.
- [7] O.R. Evans, W. Lin, *Acc. Chem. Res.* 35 (2002) 511.
- [8] E.Q. Gao, S.Q. Bai, Z.M. Wang, C.H. Yan, *J. Am. Chem. Soc.* 125 (2003) 4984.
- [9] M. Shmilovits, Y. Diskin-Posner, M. Vinodu, I. Goldberg, *Cryst. Growth Des.* 3 (2003) 855.
- [10] M. Eddaoudi, J. Kim, N. Rosi, D. Vodak, J. Wachter, M. O'Keeffe, O.M. Yaghi, *Science* 295 (2002) 469.
- [11] R. Kitaura, K. Seki, G. Akiyama, S. Kitagawa, *Angew. Chem., Int. Ed.* 42 (2003) 428.
- [12] P. Ayyappan, O.R. Evans, W. Lin, *Inorg. Chem.* 40 (2001) 4627.
- [13] S.R. Batten, *CrystEngComm* 3 (2001) 67.
- [14] G.R. Desiraju, *Angew. Chem., Int. Ed. Engl.* 34 (1995) 2311.
- [15] A.M. Beatty, *Coord. Chem. Rev.* 246 (2003) 131.
- [16] M. Eddaoudi, H. Li, O.M. Yaghi, *J. Am. Chem. Soc.* 123 (2000) 1391.
- [17] D. Sun, R. Cao, Y. Liang, Q. Shi, W. Su, M. Hong, *J. Chem. Soc., Dalton Trans.* (2001) 2335.
- [18] C.S. Hong, S.K. Son, Y.S. Lee, M.J. Jun, Y. Do, *Inorg. Chem.* 38 (1999) 5602.
- [19] J.-R. Galán-Mascarós, J.-M. Clemente-Juan, K.R. Dunbar, *J. Chem. Soc., Dalton Trans.* (2002) 2710.
- [20] R. Robson, *J. Chem. Soc., Dalton Trans.* (2000) 3735.
- [21] H.W. Roesky, M. Andruh, *Coord. Chem. Rev.* 236 (2003) 91.
- [22] H. Thakuria, G. Das, *Polyhedron* 26 (2007) 149.
- [23] H. Thakuria, B.M. Borah, G. Das, *Eur. J. Inorg. Chem.* (2007) 524.
- [24] Liu, H.X. Shao, M. Jia, X. Jiang, Z. Li, G. Chen, *Tetrahedron* 61 (2005) 8095.
- [25] C.H.L. Kennard, E.J. O'Reilly, G. Smith, T.C.W. Mak, *Aust. J. Chem.* 38 (1985) 1381.
- [26] SMART, SAINT and XPREP, Siemens Analytical X-ray Instruments Inc., Madison, Wisconsin, USA, 1995.
- [27] G.M. Sheldrick, *SADABS: Empirical Software for Absorption and Correction*, University of Gottingen, Gottingen, Germany, 1999–2003.
- [28] G.M. Sheldrick, *SHELXS-97*, University of Gottingen, Germany, 1997.
- [29] K. Nakamoto, *Infrared and Raman Spectra of Inorganic and Coordination Compounds*, 5th ed., Wiley, New York, 1997.
- [30] N. Reddig, D. Pursche, A. Rompel, *Dalton Trans.* (2004) 1474.
- [31] J.A. Schlueter, U. Geiser, J.L. Manson, *Acta Cryst.* (2003) C59, m1.
- [32] A.J. Hanss, A. Beckmann, H.-J. Kruger, *Eur. J. Inorg. Chem.* (1999) 163.
- [33] B.L.F. Szczechura, J.G. Muller, J.G.C.A. Bessel, R.F. See, T.S. Janik, M.R. Churchill, K.J. Takeuchi, *Inorg. Chem.* 31 (1992) 859.
- [34] S.B. Teo, S.G. Teoh, M.R. Snow, *Inorg. Chim. Acta* 107 (1985) 211.
- [35] C.H. Ng, S.B. Teo, S.G. Teoh, J.P. Declercq, *J. Coord. Chem.* 55 (2002) 909.
- [36] A.W. Addison, T.N. Rao, J. Reedijk, J. van Rijn, G.C. Verschoor, *J. Chem. Soc., Dalton Trans.* (1984) 1349.
- [37] W.S. Durfee, C.G. Pierpont, *Inorg. Chem.* 32 (1993) 493.
- [38] B.J. Hathaway, D.E. Billing, *Coord. Chem. Rev.* 5 (1970) 143.
- [39] R.J.H. Clark, C.S. Williams, *Inorg. Chem.* 4 (1965) 350.
- [40] M. Suzuki, A. Uehara, *Bull. Chem. Soc. Jpn.* 57 (1984) 3134.
- [41] J.P. Costes, J.P. Laurent, J.M.M. Sanchez, J.S. Varela, M. Ahlgren, M. Sundberg, *Inorg. Chem.* 36 (1997) 4641.
- [42] F.A. Cotton, G. Wilkinson, *Advanced Inorganic Chemistry*, 5th ed., Wiley, New York, 1988.
- [43] T. Yamada, T. Takai, O. Rhode, T. Mukaiyama, *Chem. Lett.* (1991) 1.
- [44] G. Das, R. Shukla, S. Mandal, R. Singh, P.K. Bharadwaj, J.V. Hall, K.H. Whitmire, *Inorg. Chem.* 36 (1997) 323.
- [45] E. Bouhlel, P. Laszloa, M. Levert, M.T. Montautier, G.P. Singh, *Tetrahedron Lett.* 34 (1993) 1123.
- [46] J.M. Brégeault, M. Vennat, L. Salles, J.Y. Piquemal, Y. Mahhaa, E. Briot, P.C. Bakala, A. Atlamsani, R. Thouvenot, *J. Mol. Catal. A: Chem.* 250 (2006) 177.
- [47] J. Haber, T. Mlodnicka, J. Pokowicz, *J. Mol. Catal.* 54 (1989) 451.